







EBBINNOT: A Hardware-Efficient Hybrid Event-Frame Tracker for Stationary Neuromorphic Vision Sensors

Deepak Singla* , Vivek Mohan* , *Member, IEEE*, Tarun Pulluri , Andres Ussa ,
Pradeep Kumar Gopalakrishnan , *Senior Member, IEEE*, Bharath Ramesh , *Member, IEEE* and
Arindam Basu , *Senior Member, IEEE*

Abstract—Conventional vision sensors are ubiquitously used around the world for internet of things (IoT) applications. As an alternative sensing paradigm, neuromorphic vision sensors (NVS) have been recently explored to tackle scenarios where conventional sensors result in high data rate and processing time. This paper presents a hybrid event-frame approach for detecting and tracking objects recorded by a stationary neuromorphic sensor, thereby exploiting the sparse NVS output in a low-power setting for traffic monitoring. Specifically, we propose a hardware efficient processing pipeline that optimizes memory and computational needs that enable long-term battery powered usage for IoT applications. The usage of NVS gives the advantage of rejecting background while it has a unique disadvantage of fragmented objects due to lack of events generated by smooth areas such as glass windows. To exploit the background removal, we propose an event-based binary image (EBBI) creation that signals presence or absence of events in a frame duration. This reduces memory requirement and enables usage of simple algorithms like median filtering and connected component labeling (CCL) for denoise and region proposal (RP) respectively. To overcome the fragmentation issue, a YOLO inspired neural network based detector and classifier (NNDC) to merge fragmented region proposals has been proposed. Finally, a simplified version of the Kalman filter, termed overlap based tracker (OT), exploiting overlap between detections and tracks is proposed with heuristics to overcome occlusion. The proposed pipeline is evaluated with more than 5 hours of traffic recording spanning three different locations on two different NVS (DAVIS and CeleX) and demonstrate similar performance. Compared to existing event-based feature trackers, our method provides similar accuracy while needing $\approx 6\times$ less computes. To the best of our knowledge, this is the first time a stationary NVS based traffic monitoring solution is extensively compared to simultaneously recorded RGB frame-based methods while showing tremendous promise by outperforming state-of-the-art deep learning solutions. The traffic dataset is publicly made available at: nusneuromorphic.github.io/dataset/.

Index Terms—Neuromorphic vision, Event-based sensor, Region Proposal, Neural Network, Tracking, Low-power

List of Abbreviations- NVS: Neuromorphic Vision Sensor, IoT: Internet of Things, DL: Deep Learning, EBBI: Event-based Binary Image, COTS: Commercial off-the shelf, KF: Kalman Filter, NN-Filter: Nearest Neighbor Filter, OT: Overlap based Tracker, EBMS: Event-based Mean Shift, RP:

D. Singla is currently with the Department of Bioengineering, University of California, Los Angeles

V. Mohan, P. Gopalakrishnan are with the School of EEE, Nanyang Technological University, Singapore

T. Pulluri, A. Ussa, and B. Ramesh are with the N.I Institute for Health, National University of Singapore, Singapore

A. Basu is currently with the Department of EE, City University of Hong Kong and was with NTU, Singapore earlier.

*D. Singla and V. Mohan are co-first authors

Region Proposal, AER: Address Event Representation, HIST: Histogram, CCL: Connected Component Labeling, ANN: Artificial Neural Network, CNN: Convolutional Neural Network, VOT: Visual Object Tracking, 1B1C: 1-bit 1-channel image, 1B2C: 1-bit 2-channel image, SC: Superior Colliculus, BB: Bounding Box, NNDC: Neural Network Detector plus Classifier, GT: Ground Truth, IoU: Intersection-over-Union, AUC: Area under Curve, NMS: Non-maximal Suppression, RGB: Red Green Blue

I. INTRODUCTION

NEUROMORPHIC vision sensors (NVS) operating on a retina-inspired principle provide advantages of ideal sampling due to change detection driven sensing, low data rates, high dynamic range and high effective frame rate [1]–[3]. It has largely been touted to be useful for high speed tracking due to microsecond resolution of events [4]–[8]. However, many practical applications from the field of internet of things (IoT) such as traffic monitoring do not require very high speed of tracking—rather, it is more important to reduce false positives. Additionally, event driven tracking requires very stringent denoise operations to reduce false positives—often found to be quite difficult to achieve. While NVS does reduce the data rate, it is also necessary to develop a full processing pipeline of low complexity operators that can result in energy efficient hardware for deployment in IoT. Current event-based processing algorithms often require a significant amount of memory and processing due to noise related events. Finally, no real comparisons are available so far in comparing an NVS with a regular RGB image sensor on the same application, particularly for stationary NVS. Earlier comparisons were only for moving NVS and also only for Dynamic Vision Sensor (DVS) + low-resolution, grayscale Active Pixel Sensor (APS) strategies as shown in [9], [10] while arguably high resolution RGB images might have more information for deep learning (DL) based methods. With the massive growth in DL-based visual solutions, it is essential to ask the question of how well does an NVS perform in object detection and tracking as compared to regular camera output processed by DL algorithms.

In this work, we show that in applications such as traffic monitoring with stationary NVS, the change detection property of NVS can enable high accuracy detection and tracking when combined with simple DL techniques of much less complexity than conventional ones [11]. In particular, we propose a new processing pipeline for stationary neuromorphic cameras that involve:

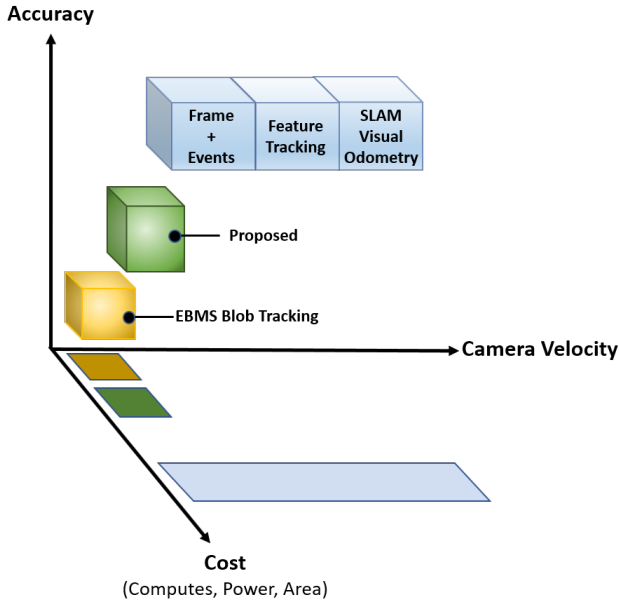


Fig. 1: A generic overview of our proposed work in comparison to other trackers for NVS data. The proposed work is less computationally complex than event-based algorithms for optical flow based feature tracker as in [15] or visual odometry [16], while tracking with accuracy much higher than cluster trackers [7] for stationary NVS scenario.

- A novel hybrid approach of creating event-based binary image (EBBI) involving time collapsing and intensity quantization of event stream. This also enables duty cycled operation of the NVS making it compatible with commercial off-the-shelf (COTS) hardware such as microcontroller units (MCU) and FPGA for IoT that rely on duty cycling for reducing energy.
- The use of simple frame-based filtering techniques for denoising the EBBI, with noise suppression comparable to conventional event-based noise filtering approaches such as NN-filter [12], [13], sometimes also referred to as background activity filter. These denoised EBBI frames require lower memory, making them suitable for implementation while simplifying the detection and tracking components in the proposed pipeline.
- Superior colliculus (SC) [14] inspired high accuracy object localization and region proposal, implementing connected component analysis on spatially down-sampled, low-resolution images.
- A hybrid neural network based detector-classifier (NNDC) flow for merging fragmented object bounding boxes and object aware false positive suppression caused by EBBI frame generation. The NNDC rectified bounding boxes can then be fed to a tracker.
- The overlap based tracker (OT) which is a computationally less intensive simplification of traditional Kalman Filter (KF) for EBBI, combining rule-based heuristics with KF like prediction and correction approach.

Since our proposed solution combines EBBI, NN based region proposal and OT for tracking, we refer to it as EBBINNOT. Figure 1 puts our work in the context of other reported works for tracking using NVS data. Some event-based

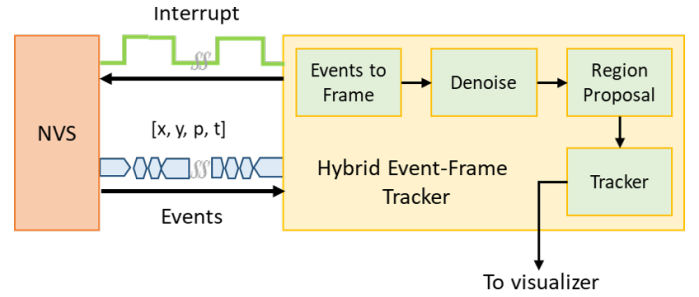


Fig. 2: Generalized block diagram for EBBINNOT

methods proposed for tracking output of NVS, such as cluster trackers [7] are very computationally cheap but the accuracy is not very high even for stationary NVS scenario. On the other hand, more sophisticated methods such as those used for optical flow [15] or SLAM [16] are very accurate in tracking even for moving NVS but with orders of magnitude increase in computations. The method proposed in this paper strikes a compromise with computational complexity close to cluster trackers but accuracy close to the best event-based trackers for stationary NVS. We use estimates of memory and computes for different algorithms to compare their hardware complexity in this work, in the absence of actual implementations.

Figure 2 shows a block diagram of EBBINNOT depicting the major blocks in the processing pipeline as well as the possibility of duty cycled interface with a NVS. It is to be noted that such hybrid approaches are becoming popular recently [17] and supporting hardware solutions are also being released [18]. An earlier version of this work was presented in [19]—however, the histogram region proposal used in [19] suffered from inaccurately sized and fragmented regions.

The rest of the paper is organized as follows. Section II describes the proposed algorithms in EBBINNOT. Section III presents the performance and computation complexity of each block as well as the whole pipeline and compares them with relevant baselines such as histogram based region proposal (HIST RP), Kalman filter (KF) based tracking, pure event-based mean shift (EBMS) tracking [7], and pure RGB frames followed by DL-based tracking. This is followed by a section that discusses the main results and also shows that our approach is NVS independent and yields expected results with two commercially available NVS: DAVIS [20] and CeleX [21]. Finally, we conclude in the last section.

II. MATERIALS AND METHODS

NVS or event camera, unlike traditional image sensors with fixed frame rate, operates by detecting temporal contrast (or change in log-intensity) at all pixels in parallel. If the change is larger than a threshold, it generates an asynchronous digital pulse or spike or event with a timestamp and a pixel location associated to it. Further, a polarity is assigned to each and every event according to the direction (increase or decrease) of contrast variation. This type of signalling is referred to as address event representation (AER). These changes in the format of data produced hence require a paradigm shift in the algorithms required for processing the input for various applications, opening up a whole new avenue in engineering [1], [3].

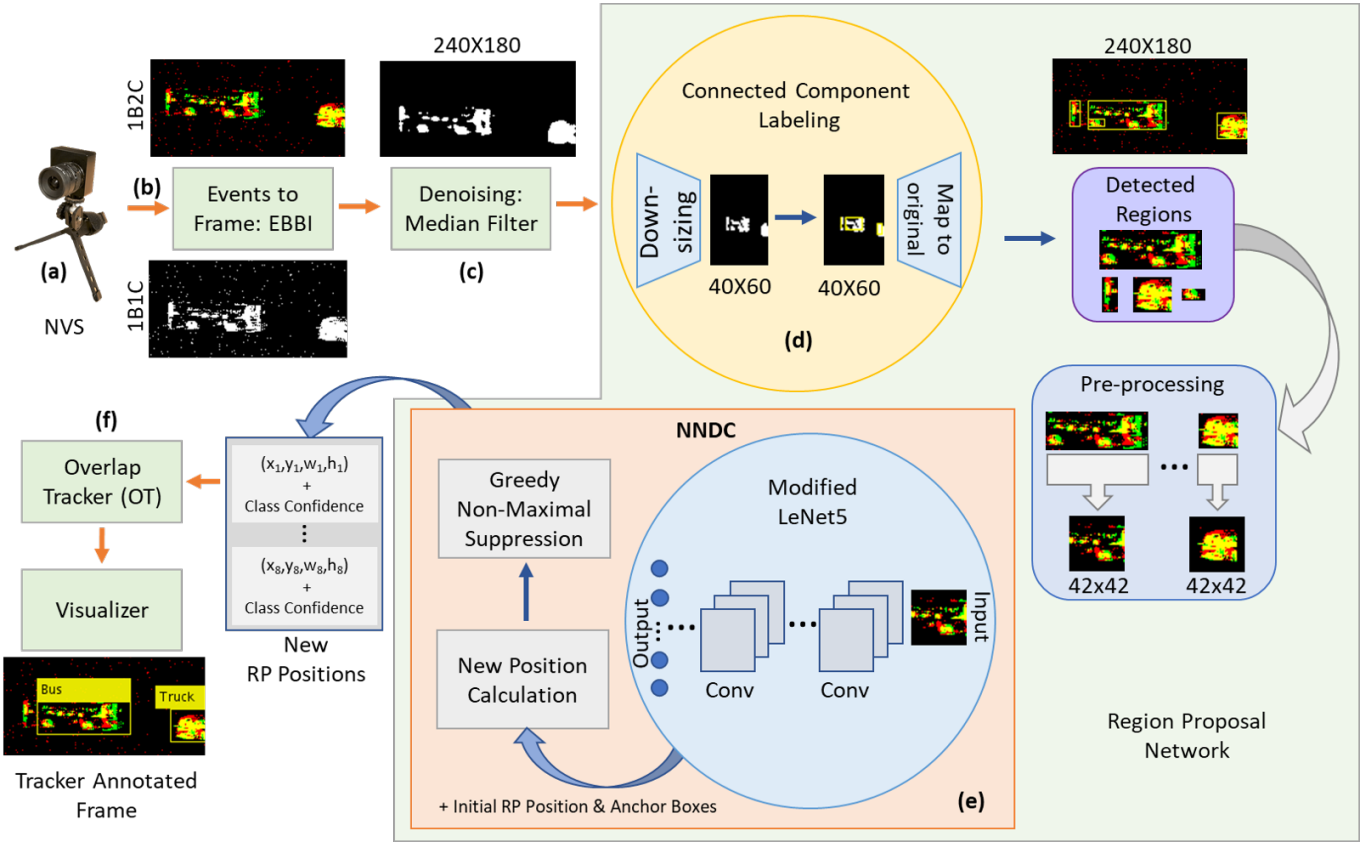


Fig. 3: Detailed block diagram of the EBBINNOT pipeline for 240×180 sensor like DAVIS. For larger sensor like CeleX, the image was downsampled appropriately by dropping lower address bits of the events, thus mapping multiple sensor pixels to same image location. Input events from the (a) NVS is converted to a binary image in (b) EBBI module (ON and OFF events in 1B2C is shown by two different colours) followed by (c) median filtering for noise removal. The region proposal (RP) consists of (d) connected component labelling and (e) NNDC blocks. The last block is the (f) tracker

Mathematically, an event can be modeled as $[e_i = (x_i, y_i, t_i, p_i)]$ where (x_i, y_i) represents the event location or address on the sensor array, t_i represents the timestamp of the event and p_i represents the polarity associated to it [22]. The associated timestamps to each event have microsecond resolution with quick readout rates ranging from 2 MHz to 1200 MHz. The event camera has an in-built invariance to illumination, since it detects temporal contrast change largely cancelling out the effect of scene illumination. In short, the variation in log intensity represents the variation in reflectance due to the movement of the objects in the view.

The proposed EBBINNOT system comprises of three major blocks (Fig. 3): EBBI and noise filtering, region proposal network (RPN) and tracking described in details below.

A. Event Data Pre-processing

1) *Event-Based Frame Generation*: In this work, we propose to aggregate events occurring within a specified time-interval (denoted by t_F for frame time) into two types of temporally collapsed images. First, a *single channel binary image* (1-bit, 1-channel image denoted as 1B1C in Fig. 3) was created by considering a pixel to be activated for any event mapping to the pixel location occurring within the interval t_F , irrespective of the polarity of the event and the event count for

that pixel location. Mathematically, we can write the equation for the (i,j) -th pixel in the k -th frame I^k as:

$$I^k(i, j) = \begin{cases} 1, & \text{if } \exists(i, j, t, p), p \in \{0, 1\}, (k-1)t_F \leq t < kt_F \\ 0, & \text{otherwise} \end{cases} \quad (1)$$

Second, a *dual channel binary image* (1-bit, 2-channel image denoted as 1B2C in Fig. 3) was obtained in the same way as in case of 1B1C, with the exception that events corresponding to two polarities are written separately, with one channel consisting of ON events and the other consisting of OFF events. Note that 1B1C can be obtained by logical OR of the two 1B2C images—however, in practice, it is better to create the two images simultaneously to avoid further delays due to memory access. These methods also minimize high frequency noise characterized by abnormal firing rates in some of the pixel similar to refractory filtering for NVS [13], [23] with refractory time t_F .

Note that this is different from the downsampling methods in [24] where the total number of events in frame duration is counted to create a multi-bit image which has been shown to be not as informative as 1B2C for classification [25]. Event-count based images may be thresholded to arrive at these EBBIs which have advantage of being hardware friendly and amenable to processing via application of simple morpho-

logical operators [26]. Akin to how visual information exits the occipital lobe into two distinct visual systems composed of *what and where pathways* [27], in our work, the region proposal network for locating the object is comparable to the *where pathway*. Finally, while the hardware implementation is a future work for us, this proposed method of EBBI allows the processor (Fig. 2) to be duty cycled since it need not count all events within the time t_F —rather, the NVS can act as a memory and retain the addresses of all events triggered in the interval till the processor wakes up, reads and resets it. Other methods of frame generation such as [28], [29] relying on fixed event count, are unsuitable when there are multiple objects in the frame with varying sizes. Lastly, we use $t_F = 66$ ms in this work, but have seen the general concept works for a range of t_F varying from 30 – 120 ms. Even lower values of t_F might be needed for tracking faster objects at the expense of power dissipation, while going to $t_F > 120$ ms led to very high motion blur in our application [30].

2) *Noise Filtering*: A conventional event-based filtering for an event stream from the NVS involves a combination of refractory filtering and an event-based background activity filter (BAF) [31] or nearest neighbouring filter (NN-Filter) which passes events occurring within a specified time interval in the neighbourhood of the event. For events in an $A \times B$ sensor dimension, represented by B_t bits per timestamp, a $p \times p$ NN-Filter, performs $p^2 - 1$ counter increments and comparisons besides a memory write for B_t bits. The total computes and memory required when NN-Filtering is performed for an average of \bar{n} events per frame was obtained as follows in [19]:

$$\begin{aligned} C_{NN-Filter} &= (2(p^2 - 1) + B_t) \times \bar{n} \\ M_{NN-Filter} &= B_t \times A \times B \end{aligned} \quad (2)$$

Note that $\bar{n} = \beta \times \alpha \times A \times B$ where $\beta (> 1)$ denotes the average number of times a pixel fires in duration t_F and α is the number of active pixels in the frame.

The creation of EBBI already provides refractory filtering as discussed earlier. It also enables us to leverage the use of median filter, a standard image processing tool, which ensures noise removal by replacing a pixel with the median value in its $p \times p$ neighborhood, while preserving the object edges [26]. Formally, the (i,j) -th pixel in the filtered image I_f can be denoted as:

$$I_f(i, j) = \begin{cases} 1, & \text{if } \sum_{n=-\frac{p-1}{2}}^{\frac{p-1}{2}} \sum_{m=-\frac{p-1}{2}}^{\frac{p-1}{2}} I(i-m, j-n) > \lfloor \frac{p^2}{2} \rfloor \\ 0, & \text{otherwise} \end{cases} \quad (3)$$

where the superscript for frame index is dropped for convenience. Mathematically, this is related to the conventional event-based noise filters in the sense that the threshold for passing an event is $\lfloor p^2/2 \rfloor$ for median filter while the same is 1 for BAF or NN-filt. Hence, our proposed method is a more stringent noise filter.

For removal of spurious noise due to pixel firing which roughly translates to salt and pepper type of noise in a 1B1C EBBI, a median filter performs an equivalent of p^2 counter increments for every 1 and $\lfloor p^2/2 \rfloor$ comparisons, besides

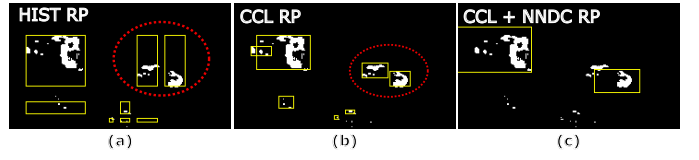


Fig. 4: Comparison of different region proposal methods: (a) HIST RP presents the problem of enlarged and fragmented bounding box due to the presence of bigger object, (b) CCL RP resolves the inaccurate bounding box issue posed by (a) however object bounding box fragmentation is still observed, (c) CCL+NNDC RP resolves fragmentation problem and removes unwanted bounding boxes

memory writes for creating the filtered EBBI. The average number of computations per $A \times B$ frame using a median filter on an EBBI is given by:

$$\begin{aligned} C_{Median-Filter} &= (\alpha p^2 + 2) \times A \times B \\ M_{Median-Filter} &= 2 \times A \times B \end{aligned} \quad (4)$$

where the memory requirement is to store the raw and filtered 1B1C EBBI frames.

With a conservative estimate of objects covering $\alpha = 10\%$ of screen area and assuming $A = 240$, $B = 180$ for DAVIS sensor [20], we obtain $C_{NN-Filter} \approx 276.4$ Kops/frame and $C_{Median-Filter} = 125.2$ Kops/frame for $p = 3$. Further, the median filter approach requires nearly $8 \times$ lesser memory than a conventional NN-filter. Lastly, we show in Section III that the performance of the EBBI with median filtering is at par with the much more expensive NN-Filter.

B. Region Proposal Networks

A crucial step to understand the visual scene involves the detection of salient visual cues, and the role of SC behind the natural vision [14], [32] is a perfect example for detection. Fundamentally, the natural vision pathway astounds researchers mostly because of its speed and efficiency, and SC proves efficient here by obtaining salient objects from a low spatial resolution version of the input [33]. Surprisingly, the low resolution achromatic images allows better performance and faster response due to less computes. Inspired by these, we propose to use a low-resolution version of 1B1C images in this work for the first phase of region proposal as described next.

1) *Move from HIST RP to CCL RP*: The projection of event information into EBBI and rejection of background by a stationary NVS provides us an opportunity to use well-known frame-based simple operators like edge detection and thresholding. To understand the context in the frame, learning the distribution of active pixels in an already foreground background separated EBBI is the key. Histogram based RP (HIST RP) explored in [19], [34], [35], extracts one-dimensional (1-D) X and Y histograms by summing up all the active pixels along the respective axis. These histogram distributions can then be easily analyzed and the consecutive entries higher than some threshold can be used to locate the probable object locations back in 2-D.

However, operating this algorithm on the image at original sensor resolution can likely yield two or more areas for the

fragmented images (e.g. glass windows in cars do not generate events and lead to fragmented clusters of events representing a car as shown in Fig. 4(a)). An appropriately chosen down-scaled version of the same image merges most of the objects. Further, a second run to weed out the false regions is done by checking the presence of active pixels in the proposed regions from the previous step. These steps still cannot help overcome the shortcoming of projecting back from 1-D to 2-D where the box for the smaller object gets affected in the presence of a bigger object (shown in Fig. 4). A tight bounding box (BB) is required for a better understanding of the object in the classification stage.

Therefore, instead of using 1-D projections, we propose to use the morphological 2-D operator like connected component labeling (CCL RP). CCL RP relies on the connectivity of a target pixel with its surrounding eight pixels, called 8-connectivity neighbours. A two-pass algorithm of CCL reviewed in [36], [37] and proposed for operation on 1B1C EBBI in [25], produces tight BBs for an effective classification process. This algorithm relies on the equivalent label in the 8-connectivity neighborhood and continuously updates the BB corners of each and every pixel using the equivalent label during its two raster scans. Applied on a downsized version of EBBI for the same reason as HIST RP, this RP also keeps the computes in control. The downsizing is also a great example of exploration of low spatial resolution saliency detection aspect of the human visual system. The downsizing is done by scaling factors s_1 and s_2 as follows:

$$I^{s_1, s_2}(i, j) = \bigvee_{m=0, n=0}^{m=s_1-1, n=s_2-1} I(is_1 + m, js_2 + n) \quad i < \lfloor A/s_1 \rfloor, j < \lfloor B/s_2 \rfloor \quad (5)$$

where $I(i, j) \in \{0, 1\}$ and s_1, s_2 are rescaling factors along X and Y axis and \bigvee represents the logical-OR operation on a patch.

The computational and memory complexity of HIST RP are reported in [19]. The corresponding equations for CCL RP labeled as C_{CCL} and M_{CCL} as derived in eq. 6, depend on the parameter α since the main comparisons in the algorithm happen only on active pixels. The first term of $C_{CCL}(M_{CCL})$ denotes the contribution of downsizing. We can keep a fixed memory assuming that we have maximum number of equivalent labels, possible only when there is an inactive pixel between every two active pixels. Therefore, the second term in M_{CCL} indicates the memory required for storing the four BB corners for each equivalent label.

$$C_{CCL} = A \times B + \alpha \frac{A \times B}{s_1 s_2}$$

$$M_{CCL} = \frac{A \times B}{s_1 s_2} + \left(\frac{A \times B}{2s_1 s_2} \lceil \log_2 \left(\frac{A}{s_1} \right) \rceil + \frac{A \times B}{2s_1 s_2} \lceil \log_2 \left(\frac{B}{s_2} \right) \rceil \right) \quad (6)$$

For our specific case, we estimated α to be between 2.7 and 4.5, by running CCL RP over the dataset as discussed later in the paper. Combining that with the sensor dimensions for DAVIS camera $A = 240$, $B = 180$ and well fitting scaling factors $s_1 = 6$, $s_2 = 3$ for our case, we estimated that HIST

RP performs $C_{HIST} = 48$ Kop/frame and $M_{HIST} = 3.44$ KB while CCL RP has maximum $C_{CCL} \approx 54$ Kop/frame ($\alpha = 4.5$) and $M_{CCL} = 16.8$ KB. Although, the number of computations are similar for both HIST and CCL RPs, the memory requirement increases five fold for CCL. However, it should be noted that such increase does not play much role in the system level since it is much less than the memory required by NNDC as shown in the following sub-section.

2) *Combining CCL and NNDC RP*: Although there are low-cost frame-based single step object detector and classifier solutions in the literature such as YOLO [11], [38], SSD-MobileNet [39], in order to target for stand-alone IoVT devices based real-time traffic monitoring, implementing such CNN based networks in compact, power-constrained hardware (< 1 mW) is not feasible.

CCL RP discussed earlier, plays a fundamental role in recognizing salient information from the achromatic binary image, but does not cover highly fragmented objects such as buses, trucks in some of the scenes generating more than two RPs for single objects (shown in Fig. 4(b)). Therefore, a secondary correction step for removing unwanted RPs and merging BBs is required. However it will require the knowledge about the RP and its associated class in order to merge them [38]. Keeping in mind the memory constraints, we propose a CNN based Detector (position correction) plus Classifier model (NNDC RP) which predicts the class and confidence for the RP, and correctly modifies the position of RP bounding box.

The initial inspiration for training this model came from YOLOv2 [38] wherein, the idea of predicting BB coordinates offsets and usage of hand-picked anchor boxes (priors) was proposed. We borrow these ideas from YOLOv2 and apply them to train a variant of LeNet5 [40], [41], with a $42 \times 42 \times 2$ input, cropped from the centroid or symmetrically zero-padded image from RP bounding box coordinates of 1B2C frame.

The network produces $C + 5$ outputs including confidences for all available classes (C), objectness score (BB_{conf}) and bounding box correction parameters (t_x, t_y, t_w, t_h). This model differs from YOLOv2 in the following aspects: (a) in place of the entire frame, the input to the model is RP obtained from CCL, (b) the anchor boxes are determined from mean sizes of class categories each representing one of the classes, unlike k-means clustering used in YOLOv2, and (c) the prediction contains just one bounding box per input RP instead of multiple bounding boxes for each grid cell of the input frame. The rest – hidden layers, activations, number of filters, filter sizes for convolution layers, in the modified model are kept the same, except for BB_{conf} and BB correction parameters which have linear activation. Physically, BB_{conf} represents whether the RP being analyzed contains sufficient information about the object or not, and a threshold (thr) to it helps in flagging the RP for rejection or consideration for passing to tracker. BB correction parameters (\hat{t}_x, \hat{t}_y) represent the predicted offset for upper left corner (RP_x, RP_y) of RP bounding box, while (\hat{t}_w, \hat{t}_h) represent the predicted width and height correction parameters for the box's width and height (RP_w, RP_h).

We note that predicting the offsets, (\hat{t}_x, \hat{t}_y) has a huge

Algorithm 1: New Position Calculation

Input : A list $[(w_i, h_i)]$, $i = 1, 2, \dots, C$, where each tuple is anchor box size for class i .
 A list $[\hat{o}_i]$, $i = 1, 2, \dots, C$, where each element is predicted confidence for class i .
 Bounding Box predicted correction parameters: $[B\hat{B}_{conf}, \hat{t}_x, \hat{t}_y, \hat{t}_w, \hat{t}_h]$
 Initial location of RP's top left corner: (RP_x, RP_y)

Output: New Region Proposal BB Location: $[\hat{x}, \hat{y}, \hat{w}, \hat{h}]$

if $BB_{conf} < thr$ **then**
 | Box is rejected;
else
 | find j , $max(\hat{o}_j)$ where $j \in 1, 2, \dots, C$;
 | for that j , get (w_j, h_j) ;
 | $\hat{x} = clip(tanh(\hat{t}_x) * (A - 1) + RP_x, 0, A - 1)$;
 | $\hat{y} = clip(tanh(\hat{t}_y) * (B - 1) + RP_y, 0, B - 1)$;
 | $\hat{w} = clip(w_j * exp(\hat{t}_w), 0, A)$;
 | $\hat{h} = clip(h_j * exp(\hat{t}_h), 0, B)$;
 | where, $clip(a, m, n)$ means a is clipped with m as lower bound and n as upper bound
end

advantage and makes the training smoother [38]. However, learning the sizes of the objects is the most important aspect for the model and therefore, we feed the knowledge of priors to the model. We ensure that the number of priors are equal to the number of classes, C , with each prior corresponding to a class. The anchor box sizes are determined from the mean sizes of ground truth (GT) BBs for each of the classes in the input dataset. The new size of RP is predicted using the anchor box size of the predicted class and size correction parameters for the RP. The complete algorithm for the calculation of corrected RP location is shown in Algorithm 1.

Model Training: While training the model, we gather all the RPs from all the training videos frame by frame and resize them into a fixed size of $42 \times 42 \times 2$, either by zero padding keeping the RP in centre or cropping it from the centroid. The true positions for each of the RPs for a particular frame are defined according to the intersection-over-union, IoU (eq. 7) with the ground truth (GT) bounding boxes for that frame. If the IoU of RP with GT box is greater than $IoU_{th} = 0.1$, the true BB_{conf} for that RP is assigned the same value as IoU and GT bounding box, $[x, y, w, h]$ act as true location for the RP; otherwise, BB_{conf} is kept 0.

$$IoU = \frac{A_{Intersection}}{A_{Union}} \quad (7)$$

where $A_{Intersection}$ is the area of intersection and A_{Union} is the area of union of RP box and the GT box. Therefore, we form the new loss function (eq. 8) combining the three components given by:

$$Loss_1 = \sum_{i=1}^C (o_i - \hat{o}_i)^2$$

$$Loss_2 = (BB_{conf} - \hat{B}B_{conf})^2$$

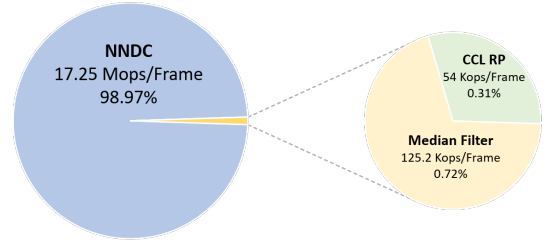


Fig. 5: Computational Cost Distribution for EBBINN on active frames (not considering temporal sparsity) assuming 8 regions proposed by CCL as input to the neural network.

if $BB_{conf} > 0.1$,

$$Loss_3 = \left(\frac{x - \hat{x}}{A - 1}\right)^2 + \left(\frac{y - \hat{y}}{B - 1}\right)^2 + \left(\frac{w - \hat{w}}{A}\right)^2 + \left(\frac{h - \hat{h}}{B}\right)^2$$

else,

$$Loss_3 = 0$$

$$Total Loss = Loss_1 + Loss_2 + \lambda * Loss_3 \quad (8)$$

where, λ is the Lagrange multiplier used to give appropriate weightage to the third component. It also helps the model to give attention to better position detection. This loss function is largely modified from YOLOv1 [42], with the penalization for BB coordinates being changed according to the IoU of RP box with the GT box, and the width and height of boxes optimized directly instead of their square roots.

While testing the model, the predicted $\hat{B}B_{conf}$ helps in rejecting the RPs and the new BB coordinates are predicted only if $\hat{B}B_{conf}$ is greater than the assigned threshold, IoU_{th} . Therefore, the knowledge of priors gives an upper-hand in predicting finely localized box and the corresponding class information. This object detector, however may be left with multiple overlapping boxes for the same object after prediction. Consequently, we suggest the application of three-step greedy non-maximal suppression (NMS) [43] for removing the unwanted overlapping boxes:

- Sort the new BBs for a particular frame according to the predicted $\hat{B}B_{conf}$.
- Start with the best scoring box and find its IoU with the other BBs one-by-one and suppress the other BB if IoU is greater than a fixed threshold, thr^{nms} .
- Repeat the same procedure with the next box in the sorted array until no extra boxes remain in the list.

It is to be pointed out that the calculation for rectified bounding box may seem unconstrained, however, the knowledge of RP being a part of the complete object allows the network to learn that the actual bounding box of required object is at a small offset of RP and has size as a factor of the prior class size.

Further, this modified version of LeNet5 has much fewer computes than other object detector models (shown in Table I). For NNDC, the average computations for a video depend on the temporal sparsity of frames, α_T , the number of RPs, n_{RP} , and can be expressed as:

$$C_{NNDC} = \alpha_T n_{RP} 2.16M \quad (9)$$

where the number of computations for running the neural network once is 2.16M. Since α_T depends on the video, we keep its value as 1 here but include actual values from

TABLE I: Computations for different object detector and classifier models

Network	Total # Computes	# Parameters
NNDC	2.16-17.3M	0.108M
Tiny YOLOv2 [38]	898M	15.74M
YOLOLite [44]	418M	0.542M
SSD-MobileNet [39]	290M	26.34M

data in Section III. Also, we choose a worst case value of $n_{RP} = 8$ and for a fair comparison with other models, we combine the computes for EBBI and CCL RP leading to a total computes bound per frame of $\approx 17.302M$ for our proposed approach as shown in Fig. 5. Note that these two blocks do not add much computes to the overall total, showing that most of the computation is done in NNDC. It can be seen that Tiny YOLOv2, YOLOLite and SSD-MobileNet have $\approx 52\times$, $\approx 24\times$, $\approx 16.8\times$ higher computes per frame respectively than this model. The computes and parameters for other models were calculated on an image size of $240\times 180\times 2$, which is the sensor dimensions of DAVIS with information in ON-OFF polarity channels.

C. Overlap based Tracking

Inspired by KF, we present a simpler tracker that takes advantage of two properties of stationary NVS: (a) rejection of background, and (b) very fast frame rates. Due to these two factors, the assignment of detections to tracks can be simplified to just checking overlap followed by greedy assignment, hence the name overlap based tracker (OT). Occlusion is handled by having extra checks based on predicted trajectories, assuming a constant velocity model. OT works on the principle of prediction of current tracker position from past measurements and correction based on inputs from the region proposal (RP) network [19]. Using P_i and T_i ($1 \leq i \leq 8$) to represent bounding boxes obtained from the region proposal network and OT respectively, each composed of upper-left corner coordinates (x,y) and object dimensions (w,h), the major steps performed by the OT for each EBBI frame, can be summarized as follows:

- 1) The tracker is initialized and the predicted position $T_i^{pred}(x, y)$ of all valid trackers is obtained by adding $T_i(x, y)$ with corresponding horizontal (V_x) and vertical (V_y) velocity.
- 2) For each valid tracker i in the *tracking* or *locked* mode, T_i^{pred} is matched with all available region proposals P_j . A match is found if overlapping area between the T_i^{pred} and P_j is larger than a certain fraction of area of the two (T_{ov}) i.e., $overlap(T_i^{pred}, P_j) > T_{ov} \implies MatchFound$ – hence the name overlap based tracker (OT).
- 3) If a region proposal P_j does not match any existing tracker and there are available free trackers, then a new tracker T_k is seeded and initialized with $T_k = P_j$. Every new tracker is initially set to *tracking mode* with no track count assigned to it. Once the new tracker matches one or more region proposals, it is set to *locked mode* and a track count is assigned to it.
- 4) If a T_i^{pred} matches single or multiple P_j , assign all P_j to it and update T_i and velocities as a weighted average

of prediction and region proposal. Here, past history of tracker is used to remove *fragmentation* in current region proposal if multiple P_j had matched.

- 5) A P_j matching multiple T_i^{pred} , can be a result of two possible scenarios—first, due to dynamic occlusion between two moving objects and second, assignment of multiple trackers to an object resulting due to region proposals corresponding to a fragmented object in the past. An occlusion is detected if the predicted trajectory of those trackers for $n = 2$ future time steps result in overlap. For tracker undergoing occlusion, T_i is updated entirely based on T_i^{pred} and previous velocities are retained. In the case of multiple matching trackers resulting from an earlier region proposal of a fragmented object, the multiple T_i^{pred} are merged into one tracker based on P_j and corresponding velocity is updated. The other trackers are freed up for future use.

Factoring the average probabilities of execution of logic sequences for different cases in the OT algorithm, the average number of computations per frame for OT, C_{OT} can be obtained as follows:

$$\begin{aligned}
 C_{OT} &= C_a + C_{oh} + C_u + C_{misc} \\
 C_a &= N_{obj}(19T_{locked} + 17T_{tracking} + 28P_1 + 37P_2 \\
 &\quad + 28P_3 + 37P_4 + 2P_5 + 2) \\
 C_{oh} &= N_{matched}(71 + 6P_6 + P_7) \\
 C_u &= 5T_{unmatched} \\
 C_{misc} &= 4
 \end{aligned} \tag{10}$$

where, N_{obj} is the average number of objects per frame, $N_{matched}$ is the average number of RPs matched to one or more trackers per frame, T_{locked} , $T_{tracking}$ and $T_{unmatched}$ are the average number of locked state, tracking state and unmatched trackers per frame respectively. P_1 and P_2 are the probabilities of tracker in locked state that are unmatched and matched to regions respectively, P_3 and P_4 correspond to the probabilities of tracker in tracking state that are unmatched and matched to regions respectively, P_5 is the probability of seeding a new tracker, P_6 is the probability of dynamic occlusion and P_7 is the probability of object matching multiple trackers but not involving occlusion. In equation 10, C_a , C_{oh} , C_u , C_{misc} represent the average number of computations performed per frame for assignment of RP to track, occlusion handling, handling unmatched trackers and some miscellaneous update operations, respectively. Numerical evaluation of this equation and comparison with KF will be done later in Section III-G. The memory requirement for implementing the OT is as low as $0.5KB$ and it can be realized using registers.

D. Tracker Class Assignment

Our work in EBBIOT [19] does not have a mechanism for assigning classes to a tracker, T_i . However, with the outputs of NNDC RP acting as input to the tracker, we resolve the problem of class assignment to the detected trackers based on the following criteria:

- If the number of matched RPs to the tracker, T_i is one, assign the same class to T_i .

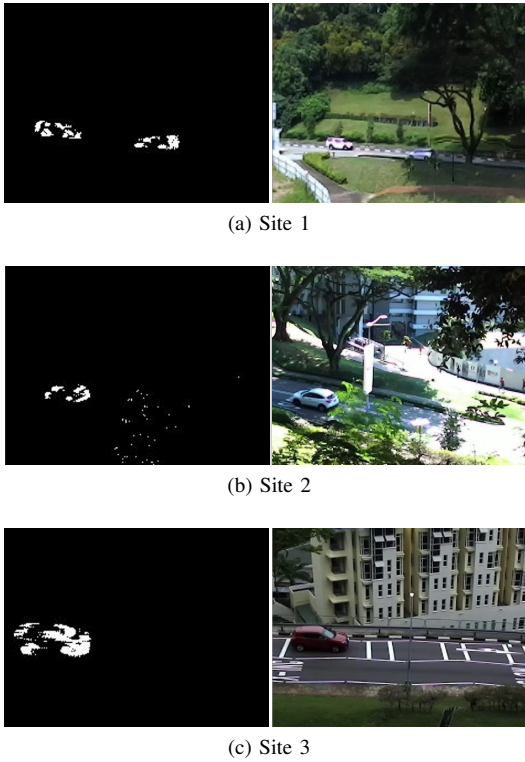


Fig. 6: Visual representation of datasets, i.e EBBI (Left) and RGB Image (Right), recorded at various sites discussed in Table II

- Otherwise, if more than one RPs are matched to T_i , select the class with highest class confidence in the combined list of class confidences of all the matched RPs. This is the new assigned class to T_i .
- If dynamic occlusion between two tracks is detected in the frame, the class assignment is stopped for both of them and these track points are not considered for voting of class for the whole track.

To summarize, the event information from NVS goes into EBBI block generating 1B1C and 1B2C images. After application of median filtering on 1B1C image, it is sent to CCL RP and then, the generated RPs are further passed to NNDC block in the form of $42 \times 42 \times 2$ images containing 1B2C image of the object. The new modified RPs from NNDC are further passed to the OT for generating the trackers along with their classification. The next section will showcase the results for the described methodology.

III. RESULTS

This section presents the data collection process followed by the evaluation of the proposed noise filtering technique. Then, we show the training of our classification model and provide insights about the hybrid RP network for the pipeline along with its comparison to other RP networks. Next, we compare the OT and KF trackers, followed by comparing the full EBBINNOT pipeline with event-based and frame-based state-of-the-art methods in Section III-F. Finally, we compare the computations and memory usage of proposed EBBINNOT with other methods.

A. Data Acquisition

In this paper, we wanted to compare performance of NVS with a standard RGB camera; however, such a dataset is not available as far as we know. Consequently, it demanded the acquisition of event-based data and RGB data from a real traffic scenario for training, validation and testing ¹.

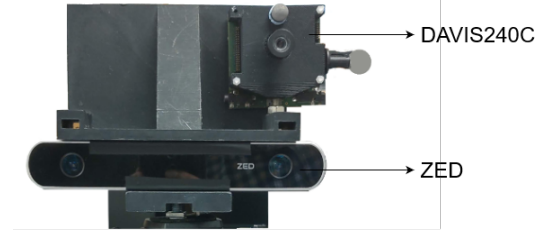


Fig. 8: Experimental setup with ZED [45] and DAVIS [20] mounted on custom-made 3D mount

The desired location for the traffic recordings was a high, perpendicular view from the road near intersections. In this regard, three places shown in Figure 6, were chosen for data collection using DAVIS. Further, we also captured RGB recordings for simultaneous comparison with the purely frame-based tracking SiamMask [46] & SiamRPN++ [47], as shown in Figure 8. For both the RGB and event datasets, manual ground truth (GT) annotation was carried out to facilitate tracker and classifier evaluation. In addition, the event and RGB data were made to have similar field-of-view (FoV) for a close comparison.

B. Evaluation Metrics

In order to test the system performance, we employed two evaluation metrics for object detection, classification and tracking.

- **F1 score for detection performance:** We have already discussed in Section II-B2 that IoU is an effective metric for evaluating the detection accuracy. The tracker annotation can be matched with GT annotation to get IoU in order to conclude whether it represents a true object BB ($IoU > IoU_{th}$) or a false object BB according to the threshold (IoU_{th}). Thereafter, we sweep IoU_{th} from 0.1 – 0.9 in steps of 0.1 to find out precision and recall averaged over the entire duration of the recording. We further calculate F1 score at each IoU_{th} as follows:

$$F1^j = 2 \frac{P^j \times R^j}{P^j + R^j}$$

$$F1^{wtd} = \frac{\sum_{j=1}^K N^j \times F1^j}{\sum_{j=1}^K N^j} \quad (11)$$

Here, P^j and R^j are precision and recall for the recording j , N^j represents number of tracks in recording j and $F1^{wtd}$ represents the weighted F1 score for all the K recordings, $j = 1, \dots, K$. Thus, we examine the detection performance of our dataset in terms of $F1^{wtd}$ swept over IoU_{th} .

¹Dataset: <https://nusneuromorphic.github.io/dataset/index.html>

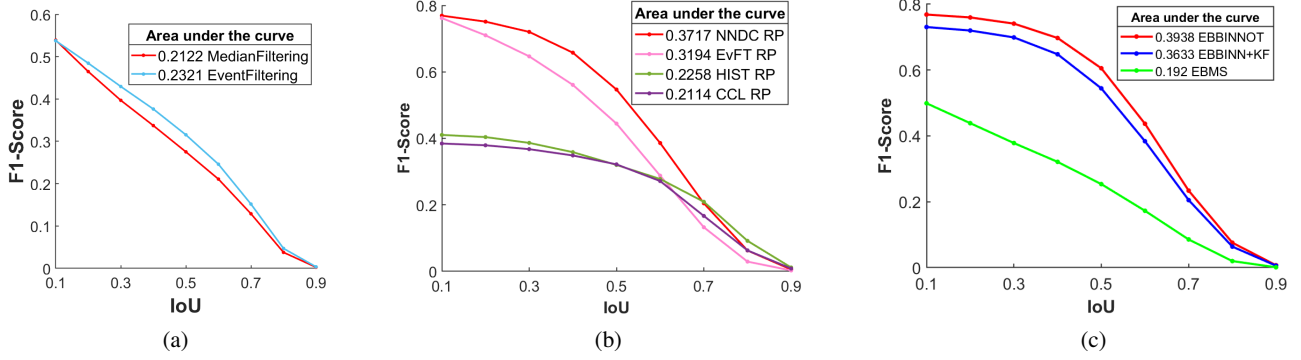


Fig. 7: Detection performance improves with each block of the pipeline, (a) Filtering Effect: Event-based filtering (Refractory Filter + NN-Filter + EBBI) Vs. Median Filtering (EBBI + Median Filter) followed by CCL RP showing comparable F1-scores with event-based filtering slightly performing superior. (b) RP Performance: NNDC (CCL+NNDC) performs much superior than others in a EBBI+RP setup. (c) Tracker Performance: Comparison between trackers show EBBINNOT to be best in terms of weighted F1-Score

- Overall accuracies for classification performance:** We calculated both the per-sample and per-track classification accuracies. In order to calculate the predicted class of a track, we recorded the statistical mode of the classification output for all the samples in the respective track of a vehicle. Further, we defined two types of accuracies: overall balanced and overall unbalanced. The former represents the average of class-wise accuracies to have a definitive evaluation measure while dealing with the dataset imbalance. The latter represents the widely used average accuracy for all the samples in the dataset regardless of class distribution.

C. Median filtered EBBI vs. Event-based noise filtering

To evaluate the effect of the proposed median filtering approach on the detection performance of the whole pipeline, we replaced it with the commonly used AER event-based nearest neighbour filtering approach [13], [48], [49]. For a fair comparison, a refractory period of $5ms$ in a neighbourhood of 3×3 was implemented for the event filtering approach, similar to the 3×3 window used for the proposed median filtering approach. Since our proposed median filter with EBBI gives on par performance with the event-based filtering approach, as shown in Figure 7(a), we advocate it for low-power hardware implementations as carried out in this work.

D. Comparison of Region Proposal Networks

Data Preparation for NNDC training: As mentioned in Section II-A1, events were aggregated at a frame rate of 15 Hz ($t_F = 66$ ms) to form 1B1C and 1B2C frames. We noted that the size of objects played a significant role for the NNDC model since an anchor box guides the class size. The objects at site 3 location had significantly different mean class sizes when compared to other sites (shown in Table III). Therefore, to facilitate the model training, we rescaled the frame by half to 120×90 at site 3 location using nearest neighbor interpolation.

Table II shows the statistical distribution of the dataset in terms of the number of samples obtained for each class category, and the number of recordings kept from each site for training and testing. The $42 \times 42 \times 2$ samples from the frames are obtained after applying CCL RP along with their correct positions, BB_{conf} and class information, by matching the respective samples with interpolated GT annotations. We also randomly selected $\approx 63,000$ noisy samples obtained from CCL RP that did not match with any GT annotations (with $IoU < 0.1$) so that the network could classify them as a separate background class and give a predicted $\hat{B}B_{conf}$ to each less than $thr = 0.1$. Assigning a different class was also necessary because these samples do not fit in any class category and in this class's absence, $Loss_1$ could not be optimized.

Note that we did not consider samples from pedestrians in the training data acquisition since they generate very few events due to their small size and slow speed. Simultaneous tracking of pedestrians and vehicles is kept as a future work. In total, we had $C = 5$ with classes: background, car/van, bus, bike and truck in our model with a total of $C + 5 = 10$ outputs. Since the buses and trucks were generally bigger than the size of 42×42 , we also included cropped samples from top-left, top-right, bottom-left and bottom-right sections of their RPs. This helped to reduce the class-wise sample variance, and also provided the information from the object's frontal and posterior region for tuned BB prediction. The bikes were augmented by random rotation within ± 15 and translation by some random amounts within the fixed area of 42×42 . The samples from recordings assigned for testing were also collected using the same criteria, but without any noisy samples having an $IoU < 0.1$. The main objective of the training was to improve the BB_{conf} , increase the BB actual overlap with the object, and also report its correct class.

Training Details: NNDC model was trained on 80% of the training data randomly selected, while the rest was kept for validation. The model was trained on an NVIDIA TITANX GPU in the form of randomly shuffled batches of 128 with

TABLE II: DAVIS traffic dataset

Recording Site	Duration	Time of Day	Lens Resolution	Number of Events	# of Recordings		Car/Van		Bus		Bike		Truck	
					in Training	Testing	(Samples Tracks)	(Samples Tracks)	(Samples Tracks)	(Samples Tracks)				
Site 1	2h11m	3PM, 4PM	12mm	201M	6	2	18232 379	8081 165	1378 35	2256 47				
Site 2	2h25m	3PM, 4PM	6mm	132M	6	3	16918 382	8019 177	1604 39	2513 56				
Site 3	1h	3PM	8mm	50M	2	1	6514 209	1201 27	512 22	501 15				

TABLE III: Mean object sizes at different recording sites

Recording Site	Car/Van	Bus	Bike	Truck
Site 1	16 × 42	31 × 94	15 × 21	22 × 50
Site 2	25 × 47	52 × 107	17 × 22	35 × 61
Site 3	34 × 82	64 × 180	26 × 44	50 × 104

TABLE IV: Classification accuracies for testing samples recorded using DAVIS

Category	per sample (%)	per track (%)
Car/Van	86.59	95.8
Bus	89.81	98.1
Bike	81.02	100
Truck	53.39	76.92
Unbalanced accuracy	85.07	95.39
Balanced accuracy	77.70	92.70

20 assigned epochs, a learning rate of 0.01 and $\lambda = 5$. This model, trained using Adam optimizer with default hyperparameters, was written in Keras framework because of the ease of writing custom loss functions like equation 8. Further, the overall unbalanced accuracy metrics on validation data after each epoch were used for early stopping of the training with patience 3. The best model was saved for evaluation on the test recordings collected at different times.

Inference: Table IV shows the per-sample as well as per-track accuracies on all the test recordings, including overall balanced and unbalanced accuracies. As expected, per track accuracies are higher due to the majority voting, and in the case of the Bike category, it is possible to get 100% classification performance. We attribute this to the unique size and shape of the bikes relative to the other categories. Overall, the balanced accuracy closely trails the unbalanced accuracy, which implies the classifier makes sound judgements instead of skewed decisions caused by the unbalanced DAVIS dataset.

EvFT RP Setup: We implemented an event feature tracker based region proposal using the feature tracker described in [15], hereby referred to as EvFT RP, so that we can compare its performance with the other region proposal schemes discussed in this work. As a pre-processing step event-based NN-Filter with a period of 5ms was used for denoising the event data. Region proposals were generated using the point cloud clustering algorithm *pcsegdist()* in MATLAB by using the coordinates of the features as well as flow information obtained from the feature tracker. In other words, features that are close together and having similar flow are grouped together in a cluster. Rectangles enclosing the clusters are used as region proposals.

Overall RP Comparison: In order to pick the best region proposal for the proposed pipeline, we ran the three RPNs, namely HIST, CCL and CCL + NNDC RP on the test dataset while restricting the maximum RPs to eight per frame. In this evaluation, the greedy NMS in NNDC had $thr^{n_s} = 0.3$ for suppressing the boxes. To compare the performance at

different *IoUs*, we used ground truth annotations at the same timestamps corresponding to the RPs.

Figure 7(b) shows the weighted F1 scores for the different RPs. Overall, the proposed CCL+NNDC RP significantly outperforms other RPs, as shown in Figure 7(b) with higher area under curve (AUC), calculated using trapezoidal numerical integration. Interestingly, HIST RP performs better than CCL RP by itself, due to lesser fragmentation by merging of overlapping regions. Integrating NNDC after CCL significantly improves this performance. Therefore, we adapt CCL+NNDC RP as part of our proposed pipeline and is also referred as hybrid RP. The closest performance is achieved by the EvFT RP generated from event-based flow computation. However, this comes at a much higher computational cost as shown later in Section III-G. It should be noted however that EvFT RP would likely perform better for situations when the camera is moving as depicted in Figure 1.

E. Comparison of Tracker

For the purpose of fair comparison of performance of different trackers, we ensured that the same region proposal network, tracker parameters, tracker log generation method and evaluation metrics were used. For comparison of KF-Tracker and OT, the number of region proposals and trackers per frame were restricted to a maximum of 8, the threshold for treating an object to be lost during tracking was set at invisibility for 5 consecutive frames or less than 60% visibility when the track is still valid. While for EBMS [7], the events were filtered using a refractory layer with period of 50ms, followed by NN-Filter with period of 5ms. The minimum number of events required for cluster formation were kept 8, maximum radius of cluster was kept 130, and a time limit of 100ms was assigned in case of inactivity of cluster. These hyperparameter values were obtained after series of runs for optimization of EBMS. Figure 9 illustrates the sample tracks generated for different types of vehicles for the trained EBBINNOT pipeline. Based on the observations made in [34], we excluded tracks for human class while calculating the F1-scores for all the 5 test dataset recordings excluding site 3.

As shown in Figure 7(c), it can be noted that OT performs slightly better than KF and significantly better than the purely event-based EBMS tracker. In order to ascertain the reason for performance improvement in OT as compared to KF, we performed an ablation study by removing specific parts of heuristics used in OT. Based on these comparisons, we can attribute the enhanced performance of OT to two reasons: first, the presence of a *tracking* mode before transitioning to *locked* state and second, the fragmentation handling logic in the OT. In our algorithm, only trackers in the *locked* state are considered as a valid track. In the KF tracker with no *tracking*

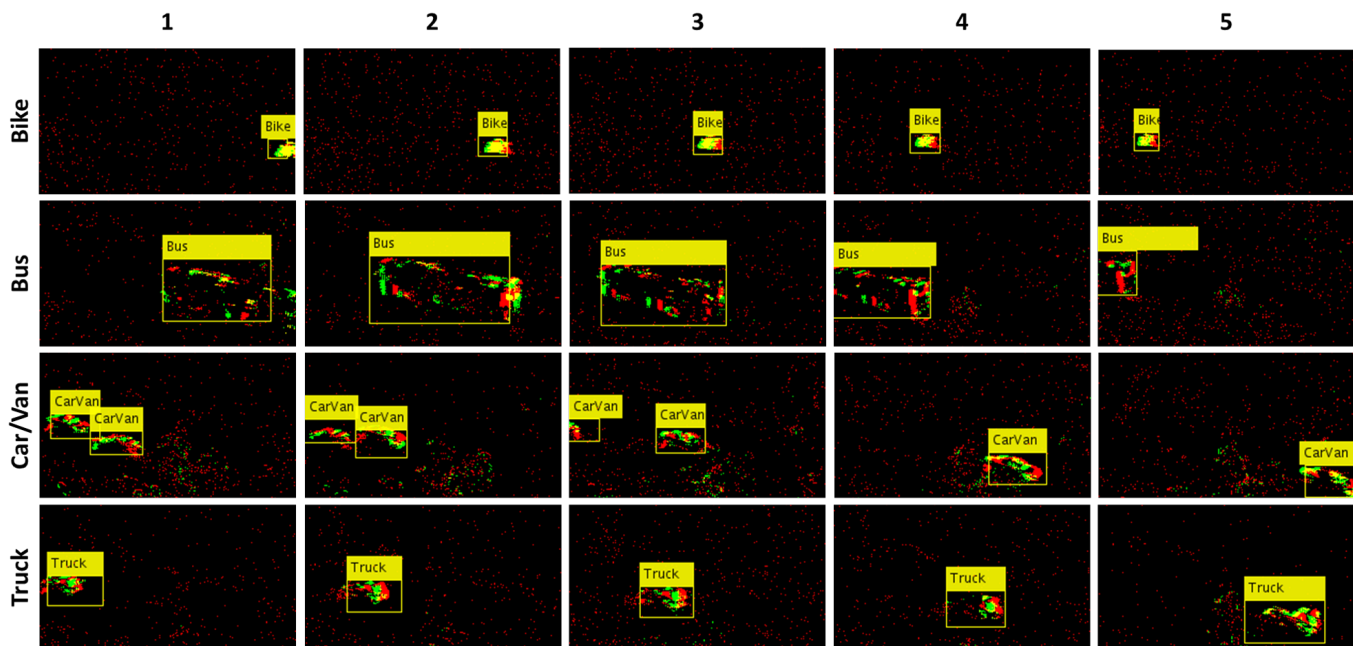


Fig. 9: Exemplar detection and classification results from the described EBBINNOT pipeline for tracks of different vehicles

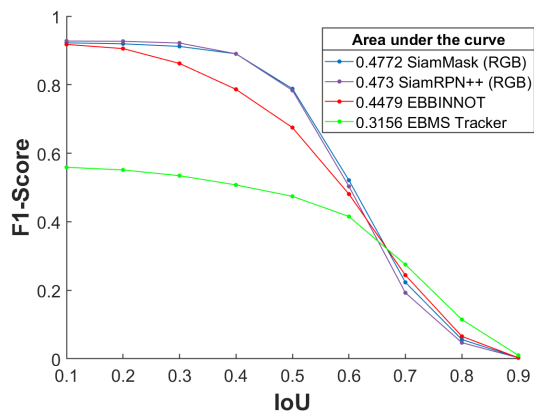


Fig. 10: Comparison of the proposed EBBINNOT, SiamMask [46], SiamRPN++ [47] and Event-Based Mean-Shift (EBMS) [7] at Site 3

mode, we observed that noisy event occurring intermittently results in false RPs creating new tracks for each of these noisy objects and increasing the false positives. As for fragmentation handling, unlike KF which cannot handle multiple trackers resulting from a fragmented object, OT utilizes past history of trackers to resolve a fragmentation in case multiple RPs match a tracker and merges multiple trackers that might be corresponding to an earlier fragmented RP, following the steps listed in Section II-C. This logic effectively reduces multiple tracks being assigned to the same object and thereby boosts the performance of OT.

F. Comparison to state-of-the-art

In this section, we report the performance of the proposed EBBINNOT compared to the frame-based state-of-the-art trackers, namely SiamMask [46] and SiamRPN++ [47], and event-based state-of-the-art approach EBMS. Since $2/3^{rd}$

of data recorded at site 3 was used to train NNDC model, as stated in Table II, we used remaining $1/3^{rd}$ of data for evaluation. Note that the original RGB dataset collected simultaneous with event-camera is used as input to SiamMask and SiamRPN++ and corresponding outputs are referred as SiamMask-RGB and SiamRPN++-RGB in this section.

Figure 10 shows the F1 scores at various IoU_{th} for test recording. Even though Siamese DNNs perform marginally better than EBBINNOT due to their inherent use of similarity matching and our provision of ground truth initialization, EBBINNOT makes use of its own RPs for tracking and can make a good case for a practical system at lower IoUs. Mainly we observed a few scenarios when the background road markings and footpath patterns of the scene became part of the RGB object representation in Siamese networks as shown in Figure. 11, causing missed tracks.

Overall, our proposed tracker comfortably outperforms the multi-object EBMS tracker while being on-par with Siamese DNN trackers. We attribute this to the need for re-scaling the frame size by half to 120×90 (previously noted in Section III-D as well), and consequently the NNDC model did not always pick a compact bounding box for some object categories. This drawback remains to be addressed in future works using techniques such as transfer learning.

G. Computational Cost

We compare the computational cost of six methods here: EBMS, EvFT, SiamMask, EBBINN-KF and the proposed EBBINNOT as shown in Figure 12.

Since our proposed OT method in Section II is closely related to KF, we detail the derivation of the number of computations per frame, C_{KF} (based on [50], [51]), for KF

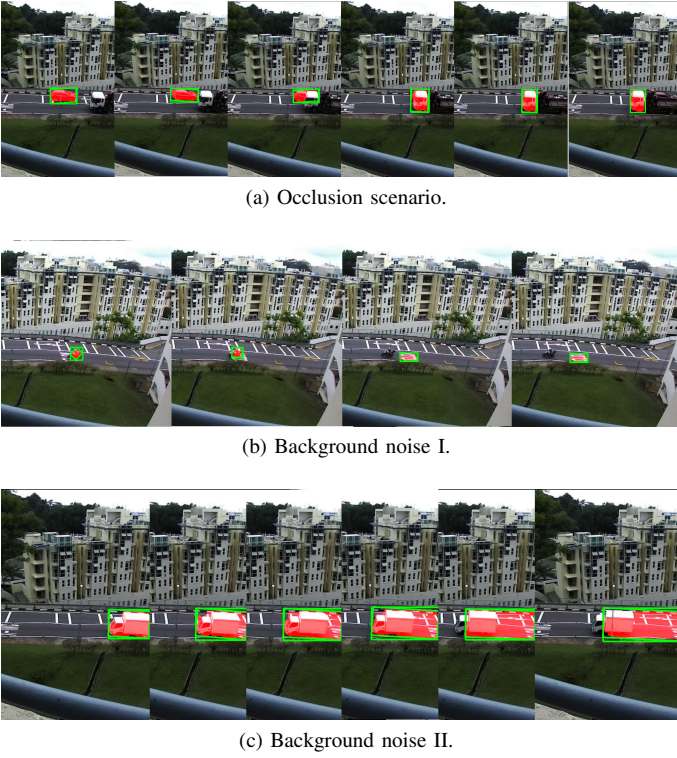


Fig. 11: Tracking performance of SiamMask under challenging scenarios. It fails to track either to background road markings or occluding objects becoming part of its online object learning representation

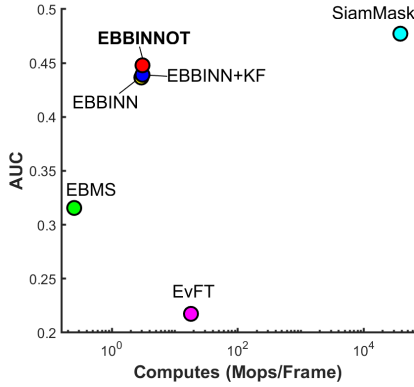


Fig. 12: Performance and computation cost comparison of the proposed EBBINNOT and other equivalent NVS trackers

Tracker as follows:

$$\begin{aligned}
 C_{KF} &= N_T(C_p + P_a C_c + P_{uat} C_u + C_{cost}) \\
 &\quad + N_{obj}(P_{ua} C_{new}) + C_{ha} \\
 C_p &= 4m^3 + 3m^2 + 2mn \\
 C_c &= 6m^3 + 6m^2n + 2mn^2 + 3m^2 + 7mn + m + n \\
 C_u &= 2, C_{new} = 1 \\
 C_{cost} &= 4n^3 + 2m^2n + 2mn^2 + 5n^2 + 5 \\
 C_{ha} &= 1/6(11N_{obj}^3 + 12N_{obj}^2 + 31N_{obj}) \quad (12)
 \end{aligned}$$

where N_T and N_{obj} are the average number of tracks and objects per frame respectively, P_a is the probability of assignment of detection to track, P_{ua} and P_{uat} are the probabilities

of unassigned detection and track respectively, and m , n are the sizes of state and measurement vectors respectively. C_p , C_c , C_u , C_{ha} , C_{cost} , C_{new} in eq. 12 represent the average number of computations per frame involved in the logic for prediction, correction, track update, Hungarian assignment, cost estimation of assignment of detection/track and seeding a new track respectively. Likewise, based on [52], we define the memory requirements for KF per frame, M_{KF} , as follows:

$$\begin{aligned}
 M_{KF} &= N_T \times WS(5m^2 + m(3n + 1) + n^2 + 2n) \\
 &\quad + (A \times B) \quad (13)
 \end{aligned}$$

where, $A \times B$ is the dimension of a binary frame and WS is the word size. Then, assuming $A = 240$, $B = 180$, $WS = 32$ and $N_T = 8$, the estimated storage needed would be approximately 6.8KB.

For the trackers, the average number of computations per frame performed by KF-Tracker (C_{KF}) and OT (C_{OT}) were estimated using eq. 12 and eq. 10 respectively, and these results were verified to be close to the actual computation count obtained by incrementing a counter with count weighted by computations in a step at run time, with an error margin of $\pm 0.01\%$. Averaged across 8 recordings at 2 sites, KF-Tracker performs $\approx 6.5 \times$ more computations as compared to the OT.

Based on the SiamMask architecture presented in [46], computations and memory usage are calculated layer-by-layer and then summed considering all network parameters and input dimensions. Total computations and memory requirements were deduced to be $\approx 38000M$ operations per frame and $\approx 157MB$ respectively.

The computations for EBBINN are obtained from Eq. 9 where the values of $\alpha_T = 0.57$ and average value of $n_{RP} = 2.38$ are estimated from the traffic dataset. It can be seen that SiamMask uses $\approx 12427 \times$ more computes per frame and demands $\approx 1450 \times$ more memory than EBBINNOT, due to its Siamese-based deep neural network architecture. Therefore, EBBINNOT offers a fair advantage in terms of total computation and memory usage.

The computes per frame for EBMS can be calculated using eq. 14, as calculated in [19].

$$\begin{aligned}
 C_{EBMS} &= \bar{N} \times [9 \bar{CL}^2 + (169 + 16 \gamma_{merge}) \bar{CL} + 11] \\
 M_{EBMS} &= 408CL_{max} + 56 \quad (14)
 \end{aligned}$$

Assuming the past 10 positions of cluster for the current velocity calculation, $CL_{max} = 8$ and for our dataset, $\bar{CL} \approx 2$, $\gamma_{merge} \approx 0.1$ and $\bar{N} \approx 650$, EBMS requires 252 kops per frame which is $12 \times$ lower than EBBINNOT, and a memory of 3.32KB, which is nearly negligible. The proposed EBBINNOT, however, significantly outperforms EBMS as shown in Figures 7(c) & 10. This performance gain comes at the cost of slightly higher computations and memory usage. Overall, out of the three approaches considered here, EBBINNOT offers the best trade off between performance and computational complexity, even though Siamese DNNs perform marginally better.

Lastly, coming to the case of EvFT RP, most computations here (over 90%) are consumed by two EM flows of the feature tracker. The RP creation process adds negligible

overhead to the tracking process. We estimated the number of computations required to implement the tracker + RP to be of the order of 1 Mops per call of the EM functions by theoretical calculation and experimental verification by profiling the MATLAB code provided in [15]. For a given recording in our dataset comprising $\approx 17M$ events spanning ≈ 16 minutes, the average number of computes per frame for EvFT is ≈ 18 Mops, which is $\approx 5.89\times$ more than that required by EBBINN.

IV. DISCUSSION

A. Repeatability of results for recordings with other NVS - CeleX

The proposed flow consisting EBBI creation, median filtering, NNDC and OT was also verified for repeatability on recordings from the CeleX [21] camera. We collected a total of 35 recordings at different times from a single location and divided them in the ratio of 5:2 for training and testing. After reviewing the size distribution of the objects from different classes obtained from the GT annotations and comparing it with the distribution from earlier recordings, we settled to resize the images by a factor of 3.33 to 384×240 from 1280×800 .

Due to the camera's invalid polarity output at some points, only 1B1C images were stored for training the NNDC model. Thus, during training and testing, the RP input to NNDC had a size of $42 \times 42 \times 1$ and the output BB coordinates were also scaled according to the new image size. We balanced the training data by augmentation and further removed the excess number of examples in classes like cars because they often appeared in the field of view.

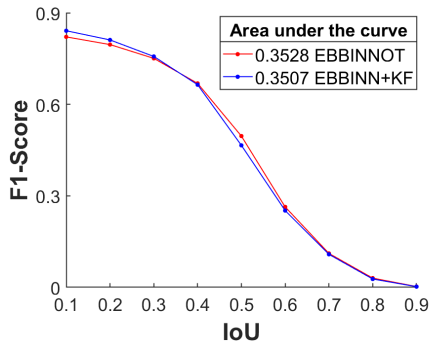


Fig. 13: Weighted F1 scores for CeleX recordings showing similar performance to the DAVIS recordings

The model was trained on the same configurations explained in Section III-D and the best model yielded the classification results shown in Table V. Moreover, the detection performance was checked after running the actual 10 testing videos on the entire setup and the generated annotations were rescaled back to the original sensor dimensions by multiplication with 3.33. We calculated the weighted F1 scores shown in Figure 13, and as expected, the performance for these recordings are comparable to the performance results of the proposed flow for DAVIS recordings, thus proving repeatability and reproducibility of the results for different recordings from different neuromorphic vision sensors.

TABLE V: Classification Scores for testing videos recorded on CeLeX

Category	per sample (%)	per track (%)
Car/Van	93.38	95.61
Bus	96.4	95.65
Bike	89.38	96.3
Truck	50.57	80
Unbalanced accuracy	91.64	95.27
Balanced accuracy	82.43	91.89

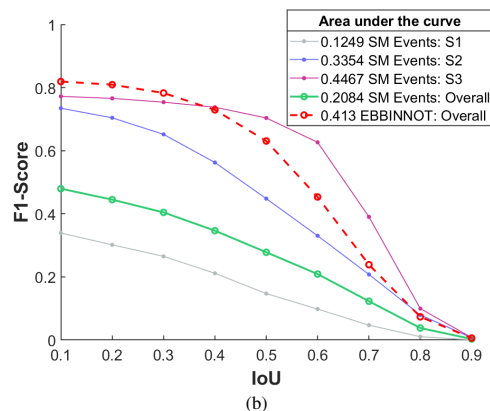
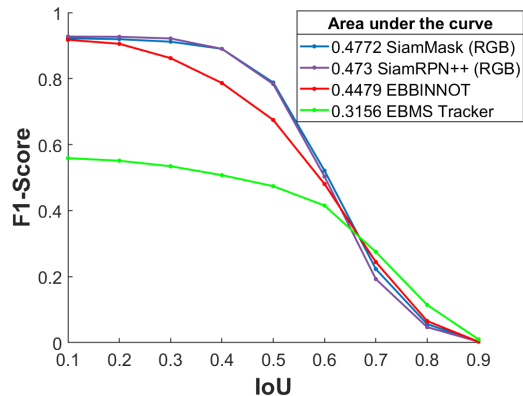


Fig. 14: (a) F1 scores of SiamMask, SiamRPN++ on Event and RGB data for site 3. (b) Weighted F1 scores of SiamMask-Events (SM Events) and EBBINNOT for different site recordings (S1, S2 and S3)

B. Analyzing Siamese DNNs with Events

In order to investigate whether the major improvement in performance of EBBINNOT comes from the background rejection property of NVS, we applied SiamRPN++, and SiamMask trackers on the EBBI directly to evaluate their performance compared to their RGB counterparts and EBBINNOT. The results obtained with EBBI as the input to SiamMask and SiamRPN++ are hereby referred to as SiamMask-Events and SiamRPN++-Events respectively. Together SiamMask-Events and SiamRPN++-Events are referred as Siamese-Events. Similarly, SiamMask-RGB and SiamRPN++-RGB are referred as Siamese-RGB.

Figure 14(a) shows F1 scores at different IoU_{th} corresponding to EBBINNOT, SiamMask-Events, SiamMask-RGB, SiamRPN++-Events, and SiamRPN++-RGB for site 3 test recordings. At lower IoU_{th} , EBBINNOT outperforms Siamese-Events, and vice versa for higher IoU_{th} . It can be

seen that Siamese-RGB outperforms Siamese-Events since RGB modality provides rich visual information about the object-of-interest in exemplar and search images for Siamese DNNs. Moreover, Siamese DNNs are designed to operate on RGB data. In case of event modality, it contains minimal information about object-of-interest in both search and exemplar images thus contributing to Siamese-Events reduced performance when compared to Siamese-RGB.

From Figure 14(b), it can be observed that size of classes at each site location is proportional to SiamMask-Events' performance. In other words for larger object size, SiamMask naturally performs better with clearer visual information. The size distribution of various objects at different sites is shown in Table III. At site 3, objects are fairly larger in size compared to the other site recordings, and thus it was chosen as final comparative evaluation for Siamese DNNs in Figure 14(a). Comparing the performance of EBBINNOT and SiamMask-Events for all site recordings, the overall performance is $2\times$ lower compared to EBBINNOT in terms of area under the curve. In summary, EBBINNOT is better compared to the deep learning-based Siamese trackers in terms of applicability and performance when evaluated on all locations, while enabling efficient hardware implementation.

V. CONCLUSION

This paper proposes a new hybrid event-frame pipeline called EBBINNOT for the IoT based traffic monitoring system using a stationary NVS. EBBINNOT creates an event-based binary image and uses median filtering to remove noise. The combination of EBBI and median filtering acts like a generalized version of nearest neighbour filtering but results in much reduced hardware cost. The output is then sent to a connected component labelling based region proposal network followed by NNDC for merging fragmented proposals, predicting their correct sizes and class categories. The modified proposals are then passed to an overlap based tracker having tracking/locked state trackers, heuristics for handling occlusion and other simplified methods inspired from Kalman Filter. All the mentioned blocks in EBBINNOT are completely optimized for computational costs. EBBINNOT requires $\approx 3.057M$ operations per frame, almost $12427\times$ less than the state-of-the-art purely frame-based Siamese DNN trackers while providing on-par performance calculated on the simultaneously collected events and RGB data. Further, this system also shows a substantial improvement over the purely events-based approach called EBMS [7] with tracking performance difference of AUC ≈ 0.14 , though requiring $12\times$ more computations. Compared to more recent event-based feature trackers [15], the proposed method requires $\approx 5.89\times$ lesser computes while delivering similar tracking performance.

EBBINNOT also achieves an overall balanced track accuracy of 92.70% on recordings from three sites spanning more than five hours. Our results show the great promise offered by neuromorphic vision sensors in monitoring applications required by IoT. Future work will focus on hardware realizations of the described pipeline and extending this work to monitoring human activity in crowded areas.

REFERENCES

- [1] C. Posch, T. Serrano-Gotarredona, B. Linares-Barranco, and T. Delbruck, "Retinomorph Event-Based Vision Sensors: Bioinspired Cameras With Spiking Output," *Proceedings of the IEEE*, vol. 102, no. 10, pp. 1470–1484, 2014.
- [2] A. Basu, et al., "Low-power, adaptive neuromorphic systems: Recent progress and future directions," *IEEE Journal on Emerging and Selected Topics in Circuits and Systems*, vol. 8, no. 1, pp. 6–27, 2018.
- [3] G. Gallego, et al., "Event-based Vision: A Survey," *CoRR*, vol. abs/1904.08405, 2019.
- [4] Z. Ni, C. Pacoret, R. Benosman, S. Ieng, and S. RÉGNIER*, "Asynchronous event-based high speed vision for microparticle tracking," *Journal of microscopy*, vol. 245, no. 3, pp. 236–244, 2012.
- [5] H. Liu, et al., "Combined frame-and event-based detection and tracking," in *2016 IEEE International Symposium on Circuits and Systems (ISCAS)*. IEEE, 2016, pp. 2511–2514.
- [6] L. A. Camuñas-Mesa, T. Serrano-Gotarredona, S.-H. Ieng, R. Benosman, and B. Linares-Barranco, "Event-driven stereo visual tracking algorithm to solve object occlusion," *IEEE transactions on neural networks and learning systems*, vol. 29, no. 9, pp. 4223–4237, 2017.
- [7] T. Delbruck and M. Lang, "Robotic goalie with 3 ms reaction time at 4% CPU load using event-based dynamic vision sensor," *Frontiers in neuroscience*, vol. 7, p. 223, 2013.
- [8] B. Ramesh, et al., "Long-term object tracking with a moving event camera." in *BMVC*, 2018, p. 241.
- [9] D. P. Moeys, et al., "Steering a predator robot using a mixed frame/event-driven convolutional neural network," in *2016 Second International Conference on Event-based Control, Communication, and Signal Processing (EBCCSP)*. IEEE, 2016, pp. 1–8.
- [10] D. P. Moeys, et al., "Pred18: Dataset and further experiments with davis event camera in predator-prey robot chasing," in *4th International Conference on Event-Based Control, Communication and Signal Processing*, 2018.
- [11] J. Redmon and A. Farhadi, "YOLOv3: An Incremental Improvement," 2018.
- [12] T. Delbruck, "Frame-free dynamic digital vision," in *Proceedings of Intl. Symp. on Secure-Life Electronics, Advanced Electronics for Quality Life and Society*, vol. 1. Citeseer, 2008, pp. 21–26.
- [13] V. Padala, A. Basu, and G. Orchard, "A Noise Filtering Algorithm for Event-Based Asynchronous Change Detection Image Sensors on TrueNorth and Its Implementation on TrueNorth," *Frontiers in Neuroscience*, vol. 12, p. 118, 2018.
- [14] B. J. White, J. Y. Kan, R. Levy, L. Itti, and D. P. Munoz, "Superior colliculus encodes visual saliency before the primary visual cortex," *Proceedings of the National Academy of Sciences*, vol. 114, no. 35, pp. 9451–9456, 2017.
- [15] A. Z. Zhu, N. Atanasov, and K. Daniilidis, "Event-based feature tracking with probabilistic data association," in *International Conf. on Robotics and Automation (ICRA)*, 2017.
- [16] A. R. Vidal, H. Rebecq, T. Horstschaefer, and D. Scaramuzza, "Ultimate SLAM? Combining Events, Images, and IMU for Robust Visual SLAM in HDR and High Speed Scenarios," *IEEE Robotics and Automation Letters*, vol. 3, no. 2, pp. 994–1001, 2018.
- [17] A. Sironi, M. Brambilla, N. Bourdis, X. Lagorce, and R. Benosman, "HATS: Histograms of Averaged Time Surfaces for Robust Event-based Object Classification," 2018.
- [18] J. Pei, et al., "Towards artificial general intelligence with hybrid Tianjic chip architecture," *Nature*, vol. 572, no. 7767, pp. 106–111, 2019.
- [19] J. Acharya, et al., "EBBIOT: A Low-complexity Tracking Algorithm for Surveillance in IoVT Using Stationary Neuromorphic Vision Sensors," *arXiv preprint arXiv:1910.01851*, 2019.
- [20] C. Brandli, R. Berner, M. Yang, S.-C. Liu, and T. Delbruck, "A 240×180 130 db 3 μ s latency global shutter spatiotemporal vision sensor," *IEEE Journal of Solid-State Circuits*, vol. 49, no. 10, pp. 2333–2341, 2014.
- [21] M. Guo, J. Huang, and S. Chen, "Live demonstration: A 768×640 pixels 200Meps dynamic vision sensor," in *2017 IEEE International Symposium on Circuits and Systems (ISCAS)*. IEEE, 2017, pp. 1–1.
- [22] C. Brandli, et al., "Live demonstration: The "DAVIS" Dynamic and Active-Pixel Vision Sensor," in *2014 IEEE International Symposium on Circuits and Systems (ISCAS)*. IEEE, 2014, pp. 440–440.
- [23] D. Czech and G. Orchard, "Evaluating noise filtering for event-based asynchronous change detection image sensors," in *IEEE/RAS-EMBS International Conference on Biomedical Robotics and Biomechatronics (BioRob)*. IEEE, 2016.

- [24] G. Cohen, *et al.*, “Spatial and temporal downsampling in event-based visual classification,” *IEEE Trans. on Neural Networks and Learning Systems*, vol. 29, no. 10, pp. 5030–44, 2018.
- [25] D. Singla, *et al.*, “HyNNA: Improved Performance for Neuromorphic Vision Sensor based Surveillance using Hybrid Neural Network Architecture,” 2020.
- [26] R. C. Gonzalez and R. E. Woods, *Digital Image Processing (3rd Edition)*. Upper Saddle River, N.J.: Prentice Hall, 2008.
- [27] P. A. Merolla, *et al.*, “A million spiking-neuron integrated circuit with a scalable communication network and interface,” *Science*, vol. 345, no. 6197, pp. 668–673, 2014.
- [28] I. Lungu, F. Corradi, and T. Delbrück, “Live demonstration: Convolutional neural network driven by dynamic vision sensor playing RoShamBo,” in *2017 IEEE International Symposium on Circuits and Systems (ISCAS)*, 2017, pp. 1–1.
- [29] J. Acharya, *et al.*, “A Comparison of Low-complexity Real-Time Feature Extraction for Neuromorphic Speech Recognition,” *Frontiers in Neuroscience*, vol. 12, p. 160, 2018.
- [30] S.-C. Liu, B. Rueckauer, E. Ceolini, A. Huber, and T. Delbruck, “Event-driven sensing for efficient perception: Vision and audition algorithms,” *IEEE Signal Processing Magazine*, vol. 36, no. 6, pp. 29–37, 2019.
- [31] T. Delbruck, “Frame-free dynamic digital vision,” in *Proceedings of Intl. Symposium on Secure-Life Electronics, Advanced Electronics for Quality Life and Society*, 2008, pp. 6–7.
- [32] R. Veale, Z. M. Hafed, and M. Yoshida, “How is visual salience computed in the brain? Insights from behaviour, neurobiology and modelling,” *Philosophical Transactions of the Royal Society B: Biological Sciences*, vol. 372, no. 1714, p. 20160113, 2017.
- [33] S. Yohanandan, A. Song, A. G. Dyer, and D. Tao, “Saliency preservation in low-resolution grayscale images,” in *Proceedings of the European Conference on Computer Vision (ECCV)*, 2018, pp. 235–251.
- [34] A. Ussa, *et al.*, “A low-power end-to-end hybrid neuromorphic framework for surveillance applications,” 2020.
- [35] S. Afshar, T. J. Hamilton, J. Tapson, A. V. Schaik, and G. Cohen, “Investigation of Event-Based Surfaces for High-Speed Detection, Unsupervised Feature Extraction, and Object Recognition,” *Frontiers in Neuroscience*, vol. 12, p. 1047, 2019.
- [36] L. He, *et al.*, “The connected-component labeling problem: A review of state-of-the-art algorithms,” *Pattern Recognition*, vol. 70, pp. 25–43, 2017.
- [37] R. Walczyk, A. Armitage, and T. D. Binnie, “Comparative study on connected component labeling algorithms for embedded video processing systems,” *IPCV*, vol. 10, p. 176, 2010.
- [38] J. Redmon and A. Farhadi, “YOLO9000: Better, Faster, Stronger,” 2016.
- [39] W. Liu, *et al.*, “SSD: Single Shot MultiBox Detector,” *Lecture Notes in Computer Science*, p. 21–37, 2016.
- [40] Y. LeCun, *et al.*, “Comparison of learning algorithms for handwritten digit recognition,” in *International conference on artificial neural networks*, vol. 60. Perth, Australia, 1995, pp. 53–60.
- [41] Y. LeCun, L. Bottou, Y. Bengio, P. Haffner, *et al.*, “Gradient-based learning applied to document recognition,” *Proceedings of the IEEE*, vol. 86, no. 11, pp. 2278–2324, 1998.
- [42] J. Redmon, S. Divvala, R. Girshick, and A. Farhadi, “You Only Look Once: Unified, Real-Time Object Detection,” 2015.
- [43] J. Hosang, R. Benenson, and B. Schiele, “Learning non-maximum suppression,” 2017.
- [44] J. Pedoem and R. Huang, “YOLO-LITE: A Real-Time Object Detection Algorithm Optimized for Non-GPU Computers,” 2018.
- [45] “Stereo Labs,” <https://www.stereolabs.com/zed/>, accessed: 2020-03-27.
- [46] Q. Wang, L. Zhang, L. Bertinetto, W. Hu, and P. H. Torr, “Fast online object tracking and segmentation: A unifying approach,” in *Proceedings of the IEEE Conference on Computer Vision and Pattern Recognition*, 2019, pp. 1328–1338.
- [47] B. Li, *et al.*, “Siamrpn++: Evolution of siamese visual tracking with very deep networks,” in *Proceedings of the IEEE/CVF Conference on Computer Vision and Pattern Recognition (CVPR)*, June 2019.
- [48] B. Ramesh, A. Ussa, L. Della Vedova, H. Yang, and G. Orchard, “Low-Power Dynamic Object Detection and Classification With Freely Moving Event Cameras,” *Frontiers in Neuroscience*, vol. 14, p. 135, 2020.
- [49] B. Ramesh, H. Yang, G. Orchard, N. Thi, and C. Xiang, “DART: Distribution Aware Retinal Transform for Event-based Cameras,” *IEEE Transactions on Pattern Analysis and Machine Intelligence*, pp. 1–1, 2019.
- [50] A. Valade, P. Acco, P. Grabolosa, and J.-Y. Fourniols, “A Study about Kalman Filters Applied to Embedded Sensors,” *Sensors (Basel, Switzerland)*, vol. 17, 2017.
- [51] J. R. Munkres, “Algorithms for the Assignment and Transportation Problems,” *Journal of the Society for Industrial and Applied Mathematics*, vol. 5, pp. 32–38, 1957.
- [52] M. Page, “Microprocessor implementation of the kalman filter,” *Microelectronics Journal*, vol. 10, no. 3, pp. 16–22, 1979.